Untersuchungen zur Strahldynamik am Harmonischen Doppelseitigen Mikrotron von MAMI-C

Dissertation

zur Erlangung des Grades
„Doktor der Naturwissenschaften“

am Fachbereich Physik, Mathematik und Informatik
der Johannes Gutenberg-Universität
in Mainz

Marco Dehn

Institut für Kernphysik
Johannes Gutenberg-Universität Mainz

13. Juni 2013

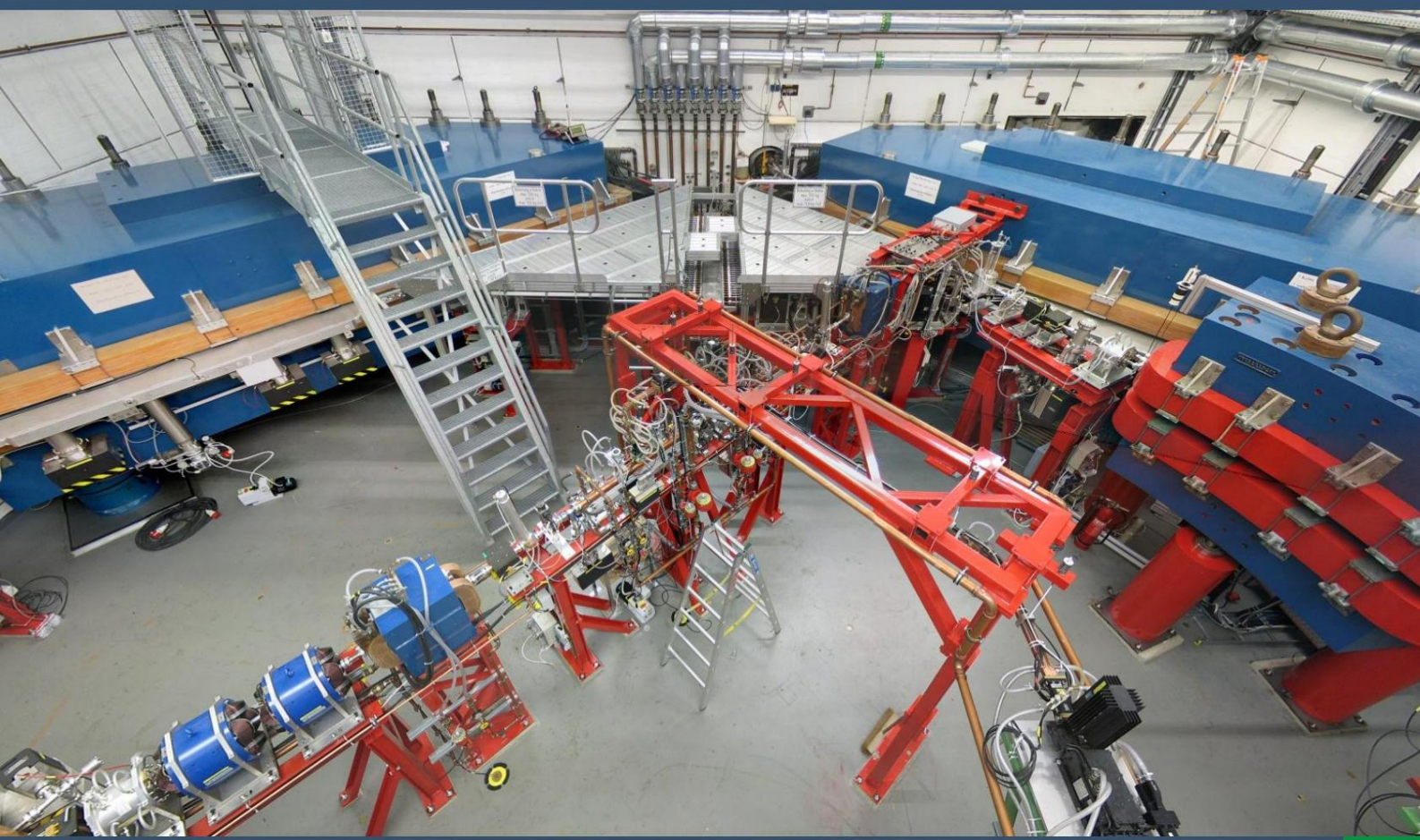

Johannes Gutenberg University, Institute for Nuclear Physics, Johann-Joachim-Becherweg 45, D-55099 Mainz

Investigations on jet dynamics Harmonic double-sided microtron from MAMI-C

Dissertation

to obtain the degree "Doctor of Science"

at the Department of Physics, Mathematics and Computer Science at the Johannes Gutenberg University in Mainz

Marco Dehn

Institute for Nuclear Physics
Johannes Gutenberg University Mainz

13th June 2013

Date of the oral exam: October 28, 2013

Summary

Since 1990, the Institute for Nuclear Physics at the University of Mainz has been operating an accelerator facility for experiments in nuclear and particle physics that is unique in the world – the Mainz Microtron (MAMI-B). This accelerator cascade consists of three racetrack microtrons (RTMs) with high-frequency linear accelerators at 2.45 GHz, with which a quasi-continuous electron beam can be accelerated from up to 100 µA to 855 MeV .

In 1999, the implementation of the last stage of expansion – a harmonic double-sided microtron (HDSM, MAMI-C) – with a final energy of 1.5 GeV began. The planning required some bold steps, such as deflection magnets with field gradients and their resulting beam-optical properties, which have a major impact on the longitudinal dynamics of the accelerator. This required the introduction of the "harmonic" mode of operation with two frequencies of the two linear accelerators.

Many machine parameters (such as HF amplitudes or phases) have a direct effect on the acceleration process, but their physical quantities are not always easily accessible by measurement. In the case of an STM with a relatively simple and well-defined beam dynamics, this is not a problem in routine operation, but with the HDSM, knowledge of the physical variables is of significantly greater importance simply because of the larger number of parameters. Within the scope of this work, it was possible to develop suitable methods of beam diagnosis with which these machine parameters can be checked and compared with the planning specifications .

Since fitting the machine model to a single phase measurement does not always provide unambiguous results due to the inevitable measurement errors, a form of tomography is used. The longitudinal phase space is then examined in the form of an acceptance measurement. An extended model can then be adapted to the variety of data obtained , resulting in a greater significance of the model parameters .

The results of these investigations show that the accelerator as a whole system behaves essentially as predicted and a large number of different configurations for beam operation are possible - however, this is avoided in routine operation and a proven configuration is used for most situations. This leads to good reproducibility, for example of the final energy or the spin polarization angle at the experiment stations.

The findings from these examinations were partially automated so that the operators now have additional and helpful diagnostics available with which the machine can be operated even more reliably.

Abstracts

The Institute for Nuclear Physics at Mainz University operates a worldwide unique accelerator for experiments in nuclear and particle physics since 1990. The Mainzer Mikrotron (MAMI-B) uses three cascaded racetrack microtrons (RTM) with RF linacs operating at 2.45 GHz to accelerate a continuous electron beam of up to 100 µA to 855 MeV.

In 1999 the realization of the fourth stage - the Harmonic Double Sided Microtron (HDSM, MAMI-C) - reaching a maximum beam energy of 1.5 GeV was started. During the development some courageous decisions were necessary. For example the bending magnets with their field gradient and corresponding beam optical properties have large influence on the longitudinal beam dynamics. That in turn requires harmonic operation with two RF linacs operating at 4.9 GHz and 2.45 GHz.

Many parameters of the machine settings (like RF voltage or phase) have great impact on the acceleration process but not always they are easily to quantify in physical units. Concerning the RTMs with their comparatively simple and well defined beam dynamics that is rather unproblematic. However, in the HDSM the larger number of parameters requires a more precise knowledge of these quantities. Therefore it is necessary to develop dedicated methods of beam diagnostics to check the important machine parameters against their design values.

All of these methods are not free of systematic errors or insufficiencies and thus fitting a model of the machine to measured data does not always yield unambiguous results. To overcome this problem a special kind of tomography is used to scan the longitudinal phase space resulting in acceptance measurements. The large amount of data with systematic variations now yields a better significance of the fitted parameters.

The results of these investigations demonstrate that the accelerator as an entity acts as predicted and shows that many different configurations can be used to operate the HDSM. However, for most situations one single configuration is established to improve the reproducibility of eg the beam energy or the spin polarization angle at the experimental areas.

Some of the resulting findings were automated to aid the operators of MAMI by means of additional diagnostic tools. These tools now guarantee a more reliable and systematic approach while operating the HDSM routinely.

Table of contents

Table of contents

Icon Directory

symbol	explanation	Unit
q, e	Charge, elementary charge Mass,	[C]
m, m0	rest mass Time, point	[kg]
t, *Ti*	in time of a revolution Voltage of the	[s]
u(t)	time-dependent signal Phase of a high-frequency	[V]
ÿ	(as specifications) Static phase shift between two	[ÿ]
ÿ = ÿ1 ÿ ÿ2	linacs	[ÿ]
ÿ	Measured phase (e.g. with phase monitors)	[ÿ]
ÿ	Phase advance of the synchrotron oscillation Working	[ÿ]
q = ÿ/2ÿ	point (“tune”) of the synchrotron oscillation Amplitude of the	
AS	synchrotron oscillation Initial phase of the	
ÿ0	synchrotron oscillation Cartesian coordinates (co-	
x, y, z	moving coordinate system)	[ÿ] [ÿ] [m]
xÿ , yÿ , zÿ	Impulses in Cartesian coordinates (moving coordinate system)	[mrad]
R	Radius of a circular path	[m]
ÿ	deflection angle	
c	speed of light speed speed	[ÿ]
v	in units of *c*	[m/s] [m/s]
ÿ = *v*/ *c*		
ÿ = ÿ1 ÿ ÿ2ÿ1	relativistic Lorentz factor	
	Wavelength of the radio frequency	[m]
ÿÿ, f	frequency of high frequency	[GHz]
ÿ	angular frequency	[Hz]
ÿ	period of high frequency	
n	efficiency	[s]
k	wavenumber	[%] [1/m]
i	jet stream	[A]
i, j, k	number of a round	
B	Magnetic field	[T]
E, ÿE, ÿE	Energy, energy gain, energy variation Peak voltage	[MeV/c2]
U0	(also amplitude) of the linac Total length of the linac *Q* (Q0,	[MV]
L	QL)	[m]
	Quality of a resonator (unloaded / loaded) rShunt = *Q*/ *Z*	
shunt impedance of a resonator	impedance of an oscillating	[Mÿ/m] [ÿ]
Z	circuit coupling constant power impulse	
k	number of linacs or	
P	deflection	[W]
p, ÿp, ÿp	systems	[MeV/c]
N	(polytron) harmonic number of the microtron	
n		
M, D, L	different transfer matrices of the longitudinal	
	beam dynamics	
Mÿ	accelerator model	
k, ÿÿ k	Accelerator configuration, configuration change	

List of abbreviations

Abbreviation	meaning	Page
MAMI	Mainz Microtron	3
RTM	race track microtron	3
DSM	Double Sided Microtron	4
HDSM	Harmonic double-sided microtron	29
DBM	"double balanced mixer" (HF mixer)	55
HF	High- frequency	4
Linac	**linear** accelerator	3
CW	"continuous wave" (continuous wave)	7
DC	direct current	56
DAC	"digital analog converter"	39
ADC	"analogue to digital converter"	58
LM	Levenberg-Marquardt algorithm	117
PSO	"Particle Swarm Optimization"	118

Part One.

Of microtrons and polytrons

Microtron, electron cyclotron, an electron accelerator similar to the ion cyclotron for energies up to about 30 MeV. The electrons travel in a vacuum chamber between the poles of a constant magnetic field on circular paths that touch tangentially at one point. At the point of contact of the circular orbits they are driven by the strong electric. Field of a microwave cavity accelerated.

Since the speed of the electrons at these energies is close to the speed of light, the orbital period changes with the energy and the orbit radius, in contrast to the ion cyclotron. Therefore, the increase in energy per revolution must be chosen so that the increase in revolution time is a multiple of the period of the microwave oscillation. Stability is achieved when the increase in energy is in turn a multiple of the rest mass of the electron. In 1944 the principle was described by V. Veksler and in 1948 the first M. by WJ Henderson, H. Le Caine and R.
Montalbetti built.

Brockhaus Encyclopedia, 17th Edition, Volume 12, 1971

Cavity resonator, an oscillating circuit for electromagnetics used in high-frequency technology.
Vibrations of very high frequency, in the simplest case a cylindrical metal can closed on all sides. You can think of it as being caused by the rotation of an ordinary oscillating circuit consisting of two parallel circular plates (capacitor) and a wire bracket (coil) around the line connecting the center points of the circle.

Brockhaus Encyclopedia, 17th Edition, Volume 8, 1971

See first, think later, then test.
But always see first.
Otherwise you will only see what
you were expecting.
Most scientists forget that.

(Douglas Adams)

1 The Harmonic Double Faced Microtron (HDSM)

The fascinating success story of the Institute for Nuclear Physics in Mainz goes back to the 1960s, when the pulsed 300 MeV linear accelerator (Linac) went into operation here [1]. Since then, major international successes have been achieved in the fields of nuclear and particle physics as well as in the field of accelerator physics, since the accelerator facility has been continuously developed to meet the requirements of the experiments [2, 3].

For the study of matter and the fundamental forces of physics, the electron is valued as an electromagnetic probe because it can be viewed as a point particle in experiments. In contrast to hadrons, where the individual momenta of the partons have to be taken into account in high-energy collisions, the entire energy Eeÿ of the electron can go directly into the collision. Therefore, investigations with an electron beam are usually easier and more precise to analyze compared to hadron beams .

1.1 The Mainz Microtron (MAMI)

In Mainz, as early as the 1970s, researchers were investigating the possibility of generalizing the racetrack microtron (RTM), consisting of *an* acceleration section and two 180ÿ deflection magnets, to *several* acceleration sections and pairs of deflection magnets in order to produce a continuous electron beam with energies well above 1 GeV for experiments of nuclear and particle physics. Beam intensities of up to 100 µA are aimed at in order to achieve high efficiency in fixed-target experiments. The generalized term *polytron1* should be used for such multi-sided microtrons with “really many” magnets [5];

1In fact, the term "polytron" in connection with plasma research and nuclear fusion was coined as early as 1961 by MG Haines ("Experiments on the Polytron, a toroidal Hall accelerator employing cusp containment") for the generation of a plasma [4].

the double-sided microtron (DSM, *N* = 2 for *two* straight segments) was initially called "bicyclotron" [6], the next higher orders would be "hexatron" (N = 3 straight segments) or "octotron" (N = 4). Figure 1.1 schematically shows the first representatives of the polytrons.

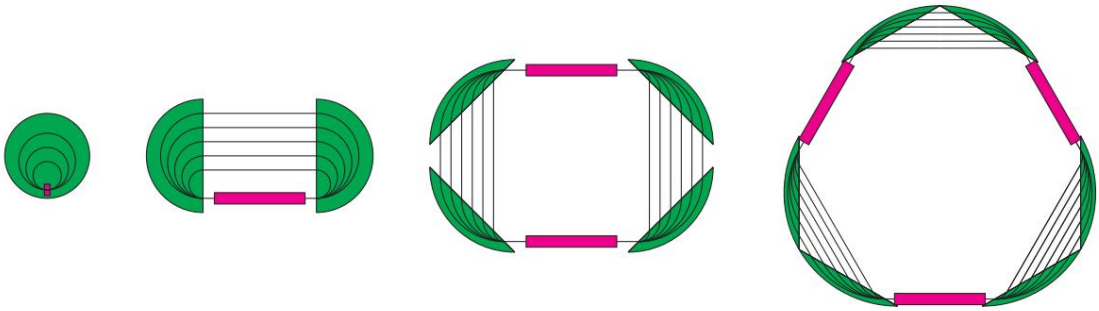

Figure 1.1:
Family of microtrons: “classic” microtron, RTM, DSM, hexatron. magnets are green HF linacs shown in purple and recirculation lanes in black (not to scale).

The fundamentally simple structure of the microtron means that just a few fundamental relationships already provide a good overview of the possibilities of the respective accelerator [5, 7]. These relationships are summarized in the following sections to understand the difficulties that were detailed during the planning. This gives rise to various questions, which are examined from Chapter 2 onwards. Chapter 3 shows how fundamental measurement results are combined to obtain additional information. In Chapter 4 in particular, the results are compared with the parameters chosen during the planning phase.

Normally, the behavior of the target particle, which crosses the accelerator on the target path, is examined. The particle experiences the target energy gain ÿESoll because it reaches the acceleration distance at the target phase ÿtarget . All other particles are characterized in the linear beam dynamics by their deviations (e.g. *ÿE, ÿÿ* or similar).

1.1.1 Recirculating RF linear accelerators for relativistic particles

The racetrack microtrons (RTM for *race track microtron)* based on an idea by Schiff [8] combine high-frequency linear accelerators (linac) with the recirculation of the relativistic electron beam through a suitable deflection magnet system. The beam can be accelerated multiple times through the linac by the energy gain *ÿE* = eULinac · cos(ÿSoll) if the recirculation flight time is an integer multiple of the accelerating HF period *ÿ* = ÿHF/c . ULinac (usually referred to as U0 in the following) is the maximum voltage of the linac and ÿSoll is the target phase of the beam

relative to the maximum HR. Since an RF linac is used, the accelerated beam cannot be continuous, but will consist of individual packets (bunches) whose maximum repetition rate usually corresponds to the RF used.

Among various other recirculating linear accelerators, the STMs play a special role: Despite the comparatively simple recirculation using two 180ÿ deflection magnets, the inherent phase focusing (Figure 1.2 and Section 1.4) of such recirculators automatically compensates for fluctuations in the energy gain *ÿE ,* since the longitudinal dispersion of the deflection system the flight time of a revolution for relativistic particles is proportional to their energy [9]. As a result, fluctuations in the energy gain do not affect the final energy as a sum, but are reduced by the number of recirculations, so that a microtron with a few recirculations will ideally have a significantly lower fluctuation in the final energy than a linac of comparable energy.

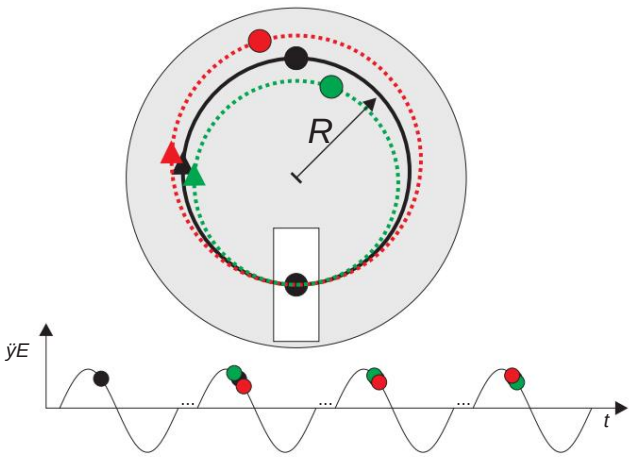

Figure 1.2:
Longitudinal focussing (phase focussing) in the "classic" microtron: In the longitudinal plane, too, the phase focussing by magnetic field (grey) and acceleration (white) ensures that particles with energy errors ÿÿ ÿ ÿ (red) and (green) reach the HF resonator later or earlier than the target particle (black). If the phase of the HF is selected in such a way that the target particle sits on the falling edge of the electric field, the energy deviations ÿÿ are compensated for within a few revolutions.

Because the electrons are already relativistic at low energies and the speed increases only slightly, a single RF linear accelerator can be used to accelerate different energies *simultaneously2 .*

2The phase speed of the accelerating high frequency *vP* must correspond to the speed of light. The target phase ÿSoll then remains practically constant during a linac passage.

Main features: deflection system and linear accelerator

The essential features of the racetrack microtron are two normally homogeneous 180ÿ deflection magnets (one can imagine the “classic” microtron divided in the middle) and an HF linac, which provides the required energy gain for the relativistic particles (Figure 1.3). As early as 1967, it was proposed to use STMs to generate a continuous high-energy electron beam for precision experiments [10].

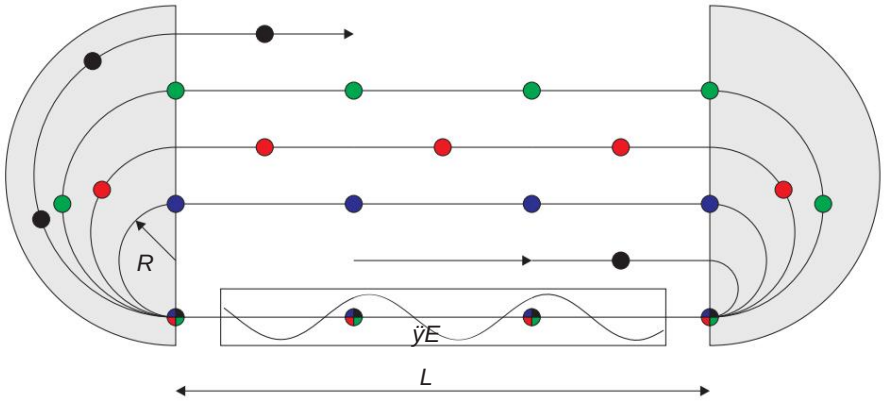

Figure 1.3:
Racetrack microtron (RTM): The magnets (grey) direct the beam or the bunches (injection, black circles) by 180ÿ into the linac. After the acceleration by ÿÿ, the deflection radius ÿ is larger (blue bunches), etc. The distance ÿ between the deflection systems can be used for the linac and focusing elements.

High energies require microtron cascade

In order for the electrons in the linac to be accelerated with each pass, they must always arrive in the resonator with the correct phase *ÿ* (coherence condition, Section 1.2.1). For this, the flight time must be an integer multiple of the HF period duration THF .
The cyclotron frequency fZ corresponds to the rotation frequency of the first rotation and thus to the minimum HF accelerator frequency in the "classic" microtron. It links energy *E* = ÿm0c2 (rest mass m0) and magnetic field B:

$$fZ = \frac{1}{2ÿ} \cdot \frac{q}{Bÿm0} \quad (1.1)$$

With a magnetic field of 1 T , a cyclotron frequency of 28 GHz results for *ÿ* = 1 . Two conclusions can be drawn from this:

1. "Slow" electrons *(ÿ* < 10) can only be meaningfully accelerated in the classic microtron with magnetic fields *B* ÿ *0.1* T in order to avoid high frequencies in the technically

being able to use the easily controllable S-band range (2-4 GHz); However, high energies are uneconomical with low magnetic fields because of the large bending radii.

2. On the other hand, highly relativistic electrons *(ÿ* ÿ 10) can also be accelerated with S-band technology, but now with magnetic fields of 1 T or more.

Taken together, both conclusions justify the construction of a cascade of microtrons to reach higher energies [11]. With the same acceleration frequency3 in the cascade, the magnetic fields of each stage are selected to match the respective energy range.

high frequency accelerator

The parameters total length L, energy gain *ÿE* and operating frequency *ÿ* of the linac can be flexibly adapted to local conditions. Normally conducting cavity resonators with an unloaded Q0 of 103 to some 104 at frequencies in the S-band are used, acceleration gradients of some 10 MV/m and more (pulsed) and around 1 MV/m (CW) can be achieved and only through the available HF power or cooling is limited, since a large part of the PHF power is dissipated in the resonators [7, 12, 13].

With the shunt impedance4 rShunt, the maximum acceleration voltage of a acceleration section can be calculated as a function of the coupled RF power:

$$U0 = ÿ\, nacc./2\, ÿHF\, rShunt\, PHF \quad (1.2)$$

nacc . the number of acceleration cells. In the case of the MAMI sections, rShunt is around 70 Mÿ/m at 2.45 GHz and around 80 Mÿ/m at 4.9 GHz. With a length of around 1 m and nacc. = 35, a power of around 15 kW is required for an energy gain of 1 MeV from the 4.9 GHz sections. Both the 2.45 GHz and 4.9 GHz klystrons deliver between 50 kW and 60 kW output power. The performance is ideal for a two meter long 2.45 GHz section or two 4.9 GHz sections

to supply.

If a beam current of 100 µA is to be accelerated with a linac, the efficiency *ÿ* = Pbeam/PHF ÿ100W/15 kW of these normally conducting structures is very small. It is therefore much more economical if the beam traverses the structure multiple times.

3The bunch repetition frequency ÿBunch of the first stage determines the minimum frequency of all following stages. Only integer multiples *k* · ÿbunch of this frequency can be used in the cascade.

4With the relationship u0 = *ÿ2pHFrShunt ,* at resonance the shunt impedance rShunt, which is determined by the geometry of a resonator, links the coupled power pHF with the peak voltage u0 of the individual resonator [14].

1.1.2 The MAMI-B cascade since 1990

The era of the pulsed linear accelerator in Mainz came to an end in 1989. More than a decade earlier, it was decided to set up a microtron cascade of three STMs that would reach an energy of 855 MeV at a beam current of 100 µA [11, 15]. The STMs, which were set up in two expansion phases, proved to be very reliable and delivered excellent beam quality: final energies of up to 855 MeV and beam intensities of up to 100 µA at 85% polarization are available in routine operation for experiments in nuclear and particle physics [16-18]. Figure 1.4 shows the current floor plan of the accelerator facility.

High beam quality of the microtron cascade

The absolute energy of the beam can be determined with an accuracy of ±160 keV by very precisely measuring the bending radius in the known magnetic field of the RTM3 bending magnet [19]. In addition, the natural relative fluctuations *ÿp/p* ÿ 10ÿ4 can be reduced to almost *ÿp/p* ÿ 10ÿ6 by measuring the energy-dependent flight time of the extracted beam through the RTM3 bending magnet using two RF phase monitors (see Chapter 2) and is stabilized accordingly [20].
The natural pulse width is about *ÿp* ÿ 12 keV at 855 MeV, which is essentially caused by the stochastic emission of synchrotron radiation quanta in the RTM3 .

1.1.3 Extension of the cascade to MAMI-C

However , the production threshold of some mesons and hyperons of nuclear physics interest requires a higher beam energy than that of MAMI-B. From around 2 GeV, the electron stretcher facility (ELSA) in Bonn could be used for complementary experiments. However, such a synchrotron is not suitable for some of the planned experiments (eg intensities over 1 µA, parity violation). Therefore, in 1999 the decision was made to increase the energy from 855 MeV to around 1.5 GeV within the framework of the newly founded Collaborative Research Center 443 of the DFG (“Many body structure of strongly interacting systems”) in order to close this gap. Here, too, the proven technology of MAMI was essentially used (ie no technological innovations such as superconducting high-frequency structures or magnets) in order not to impair the good beam quality and reliability of MAMI, even at the highest energies .

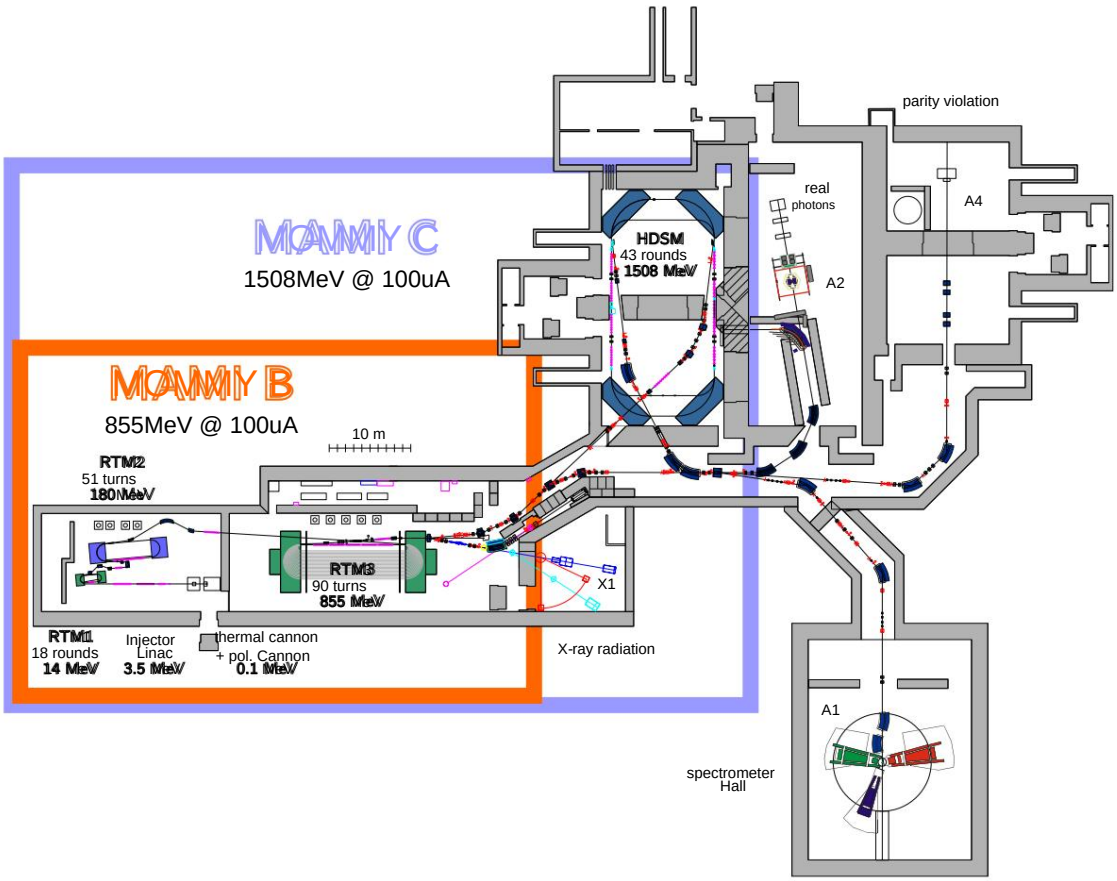

Figure 1.4:
Floor plan of the MAMI accelerator facility: MAMI-B started operations in 1990-1991 in the buildings specially built for this purpose. The beam guidance from RTM3 and the spectrometer hall were set up in parallel. The other parts of the building (HDSM, A2 and A4) date from the time of the Mainz linear accelerator and were used as experimental sites before MAMI-C. The high cost of a new, separate HDSM building led to the HDSM being constructed in two of these experimental halls (originally X1 collaboration). The X1 collaboration, in turn, moved to the smaller loading hall, which is directly adjacent to the RTM3. For all other experiments (A1, A2 and A4) all energies that can be reached with MAMI-C have been available since 2007.

No RTM4

Various arguments speak against another RTM: Because of the large magnet mass5 , the accelerator would be comparatively expensive; In addition, the relatively small energy gain means a correspondingly high number of recirculations, which above 1 GeV would also mean strongly increasing synchrotron radiation losses and an increase in the energy range.

A double-sided microtron requires only a fraction of the magnet mass compared to a comparable microtron (i.e. same magnetic field), mainly because the beam penetrates less deeply into the magnet and the pole area becomes smaller overall [7]: The magnetic area of the STM is ÿR2, for a double-sided one A microtron results in *(ÿ ÿ 2)R2,* for a hexatron *(ÿ ÿ 3/2* ÿ3)R2 etc., where *R* is the bending radius of the last revolution.
The relative saving effect on the pole face is greatest from *N* = 1 to *N* = 2, which is shown schematically in Figure 1.5.

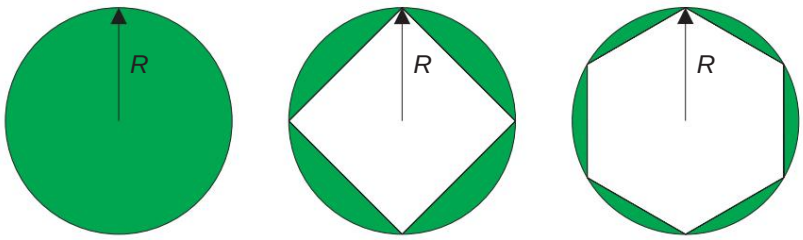

Figure 1.5:
Pole area of different types of microtrons: The pole area for a given magnetic field ÿ and energy ÿÿÿÿ is largest for the classic microtron (ÿ ÿ ÿ) with ÿÿÿ and decreases with increasing ÿ.

1.1.4 The harmonic double-sided microtron (HDSM)

The HDSM (Figures 1.6 and 1.7) is adapted to the special situation at MAMI:

- The accelerator fills the entire available space of two former experimental halls (see Figure 1.4).
- The transversal focusing can be realized with quadrupole magnets on the linac axes, as with the STMs , because the ratio between exit and injection energy is only 1508 MeV / 855 MeV, much lower than with all previous MAMI STMs.

5With a constant magnetic field, the magnetic mass scales almost with E3, so it would be from the RTM3 with 2×450 t to the RTM4 with 2×3000 t increase drastically.

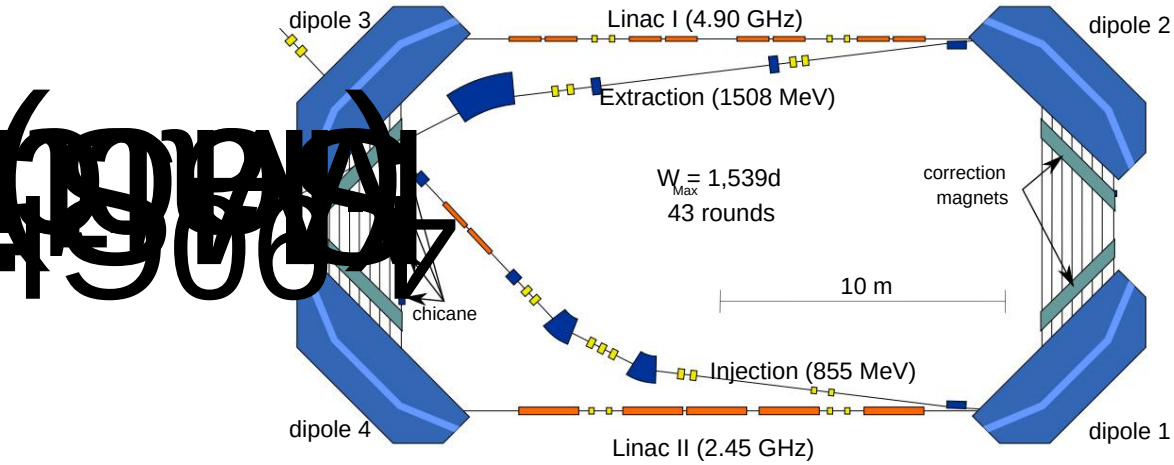

Figure 1.6:
Schematic of the HDSM: After the injection (energy matching with the matching section), two linacs (4.9 GHz and 2.45 GHz, section 1.5) accelerate the electrons. Correction magnets (each two pairs h/v) on the dispersive return paths direct each orbit centered through the following linac.
The four magnet "chicane" in the first loop between dipoles 3 and 4 lengthens the running distance to complete the longitudinal adjustment (Section 1.4.3).

The most important solution approaches of the HDSM are listed here:

- Fundamental frequency at 4.9 GHz to reduce the energy gain (section 1.2.2) • Innovative focusing scheme thanks to the field gradient of the dipole magnets to avoid the vertika master phase space (Section 1.3.1)
- This results in a migration of the target phase ÿtarget from cycle to cycle (Ab section 1.4)
- Longitudinal stability problems can be avoided by the 2.45 GHz linac (Linac II), since with subharmonic injection in a linac only every second resonator is occupied - hence the term *harmonic* DSM (Section 1.5, Figure 1.8)

In order to be able to understand how this new accelerator works, the difficulties that had to be taken into account in the design are explained in the next few sections. The RTM is often used here, which makes it easier to see some problems.

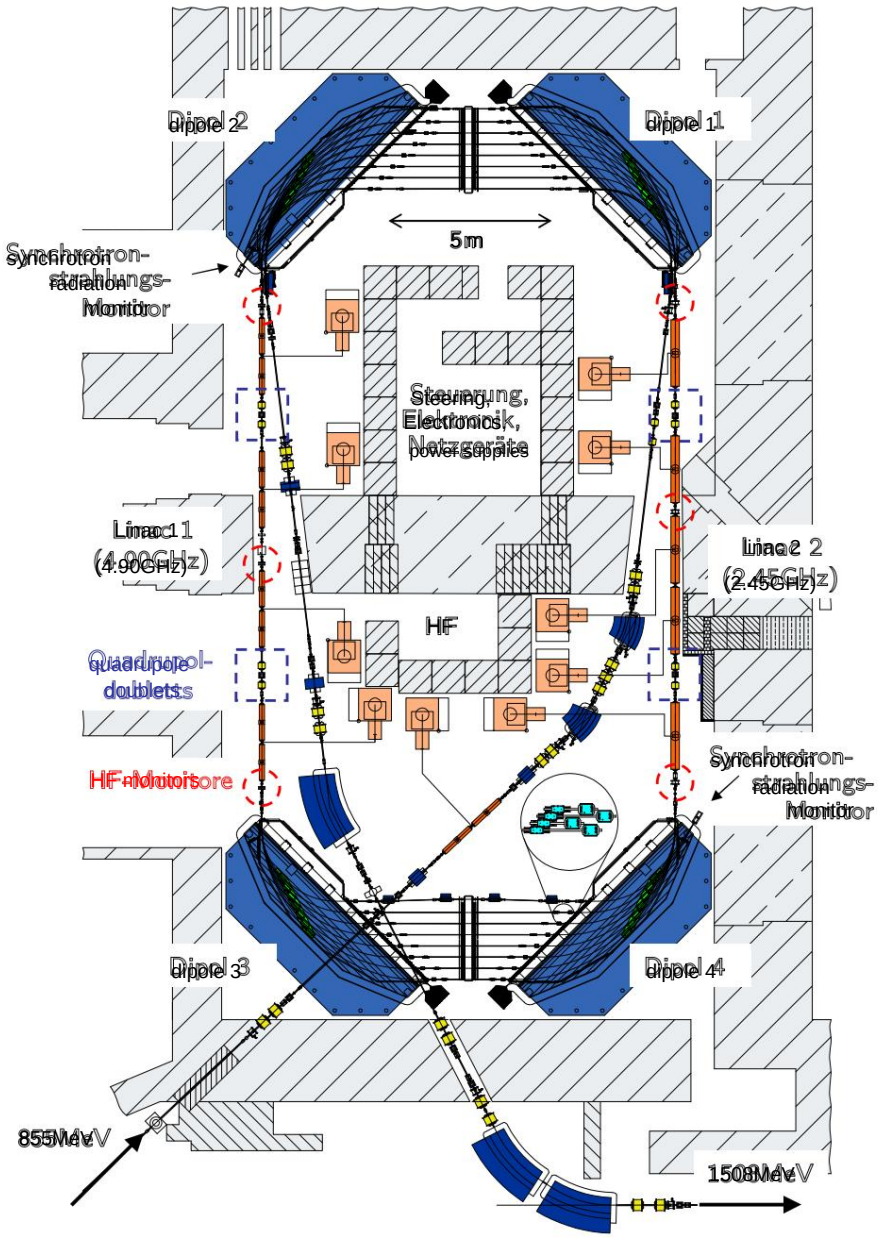

Figure 1.7:
Ground plan of the HDSM: beam diagnosis (intensity, phase, as well as ÿ and ÿ) for all orbits is realized with the HF monitors on the linac axes (red markings, details in Section 2.6), and focusing is also done exclusively with four quadrupole doublets (yellow) on the linac axes. With the 2.45 GHz linac, one klystron supplies each acceleration section; with the 4.9 GHz linac, the power of each klystron is distributed over two sections. The synchrotron monitors are used to examine the transverse properties of the beam.
In the enlarged section at dipole 4, the arrangement of the correction magnets (turquoise) on the dispersion paths is shown as an example.

1.2 The microtron principle

The basic idea behind the microtron is to use an acceleration structure (or Linac) to traverse several times and thus to use more efficiently6. In particular with normally conducting acceleration structures, the efficiency *ÿ* = PBeam/PHF is too small to economically accelerate a continuous electron beam in the GeV range.

The core components of the microtron are the acceleration structure and a deflection system common to all energies, which first separates the beams of different energies and later directs them back into the accelerator axis in phase.

The simplest example of this is the "classic" microtron (see Figure 1.2): The homogeneous magnetic field perpendicular to the accelerator level allows the electrons of different energies to return to the common starting point, where the HF resonator for acceleration is located at the same time.

The generalization of this principle replaces the circular deflection magnet of the recirculation by 2×N pairs of deflection magnets with deflection angle 180ÿ/N. Due to the arrangement in pairs, the rays are also directed onto a common axis after passing through a pair of magnets [5].

1.2.1 Coherence conditions for relativistic energies

With the microtron *(ÿ* ÿ 1), the flight time of a recirculation depends on the energy im Essentially determined by the increasing orbit radius (transversal dispersion):

$$R = \frac{\ddot{y}\,E\_}{e\,c\,B} \tag{1.3}$$

This resulting change in flight time is the longitudinal dispersion.

As early as 1944, Veksler published the following simple concept for accelerating relativistic particles (“classic” microtron):

1. The flight time of the first recirculation at energy E0 must be an integer multiple *(m* ÿ N) of the accelerating high-frequency period (static coherence condition, equation 1.4).

2. The flight times of the next recirculations at the energies *Ei* = Eiÿ1 + *ÿE* must increase by an integer multiple *(n* ÿ N) of the accelerating high-frequency period (dynamic coherence condition, harmonic number n, equation 1.5).

6Compared to a linac with the same beam energy and intensity, the cost savings in the Purchase and operation can be significant.

This corresponds to the two relations (for $\ddot{y} = 1$):

$$2\ddot{y} \frac{E0}{e \, c \, B \, \ddot{y}E} = m * \ddot{y}HF \tag{1.4}$$

$$2\ddot{y} \, e \frac{\_}{c \, B \, \_} = n * \ddot{y}HF \tag{1.5}$$

The minimum energy gain to be applied is thus determined solely by the selection of the magnetic field *B* and the HF wavelength ÿHF . With two deflection systems, each consisting of two 90ÿ deflection magnets, the relations for a complete revolution change as follows simply because of the magnet arrangement:

$$2(\ddot{y} \, \ddot{y} \, 2) \frac{\ddot{y}E}{e \, c \, B} = n * \ddot{y}HF \tag{1.6}$$

The minimum energy gain of such a "one-sided" double-sided microtron is almost three times *(2ÿ/ 2(ÿ* ÿ 2)) larger than that of an STM. If such a microtron is equipped with *two* linacs, the coherence conditions for both half revolutions must apply simultaneously, so that the path length change of a full revolution must now be at least *2ÿ :*

$$2 \, (\ddot{y} \, \ddot{y} \, 2) \frac{\ddot{y}E}{e \, c \, B} = 2n * \ddot{y}HF \tag{1.7}$$

Although the pole area of a double-sided microtron is drastically reduced, two linacs have to achieve five times the energy gain compared to an STM.

In principle, the smallest possible energy gains are preferred in CW operation (ie *n* =1); However, in order to build the accelerator as compactly as possible, the magnetic field must be as large as possible.

1.2.2 Higher energies with MAMI-C

MAMI-C should be set up in two halls previously used as an experimental area in order to save costs for a new building (see Figure 1.6). Because conventional magnets with a large homogeneous pole area *(ÿB/ B* ÿ 10ÿ4) reach maximum fields of about 1.5 T , the energy gain of a double-sided microtron should be about 40 MeV according to Equation 1.7 at the MAMI frequency of 2.45 GHz.

Consequence for MAMI-C

Both linacs would therefore have to provide a maximum acceleration voltage of U0 ÿ 25 MV – with an available length of around 12 m.

The energy gain according to Equation 1.7 is proportional to ÿHF, so it can be influenced by the choice of acceleration frequency and thus ÿHF . The MAMI-B cascade as a pre-accelerator delivers a beam with a 2.45 GHz structure, so that

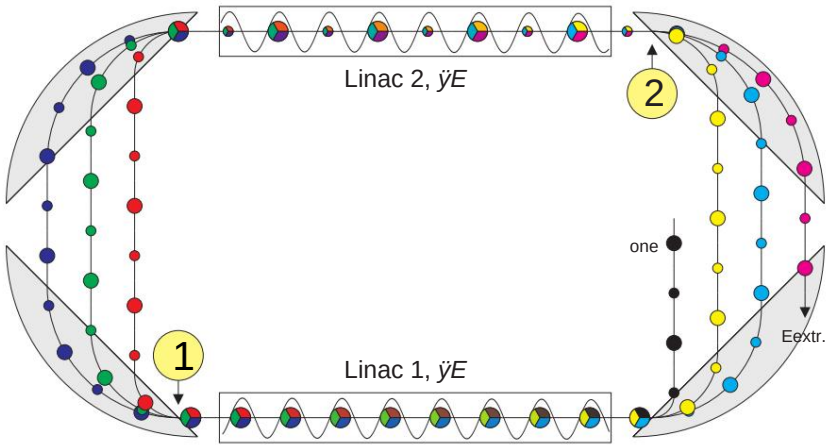

Figure 1.8:
Double-sided microtron (DSM): Schematic representation with electron bunches. From (1) to (2) the distance ÿÿÿ ÿÿÿ, from (2) to (1) is already ÿÿÿ ÿÿÿ long , since the beam energy is already greater than from (1) to (2) . The first round is therefore 37ÿ long. From (1) to (2) the route is now ÿÿÿ ÿÿÿ long , exactly 1ÿ longer than in the first round, from (2) to (1) now ÿÿÿ ÿÿÿ. Thus, the second wrap is 39ÿ long, 2ÿ longer than the first wrap, as required by Equation 1.7. Every second bunch is shown smaller because with MAMI-C (4.9 GHz) only every second bunch (ÿÿÿÿÿÿ ÿ ÿÿÿÿGHz) is occupied. Therefore, in the case of ÿ ÿ ÿ the bunches are separated by ÿ on one linac line and by 2ÿ on the other. The length of the first circuit (even /odd) determines which bunch spacing will be on which linac straight. In principle, this enables operation with two 4.9 GHz linacs (DSM) as well as mixed operation (4.9 GHz and 2.45 GHz linac, harmonic DSM, section 1.5).

initially all integer multiples of this frequency come into consideration. Because the dimensions of the acceleration structures scale with the wavelength, 4.9 GHz for the DSM is a good compromise between energy gain on the one hand and production, adjustment and, above all, aperture on the other. Figure 1.8 schematically shows the special situation with MAMI-C, which arises due to the differences in the bunch frequency and fundamental frequency of the DSM. Further details can be found in [21], for example .

1.3 The deflection system and its properties

The recirculation can be realized by segment magnets, each with common entry and exit edges (see Figure 1.9), since such a magnet has telecentric imaging properties in the deflection plane for reasons of symmetry and therefore acts like a magnetic mirror. The deflection angle remains energy- independent; only the bending radius and thus the exit point scales as transversal

dispersion with the energy. The symmetrical combination of two magnets of the same kind exactly reverses this effect of the single magnet, so that the transverse dispersion vanishes after such a deflection system and the trajectories of all energies are reunited [6]. The deflection angle of both magnets must be the same. It makes sense to use deflection angles of twice $\ddot{y}$ = 180ÿ/N, where *N* is the number of deflection systems with pairs of magnets or straight sections with dispersion *D* = 0. Possible are 180ÿ (RTM, *N* = 1), 90ÿ (DSM, *N* = 2), 60ÿ (Hexatron, *N* = 3) etc.

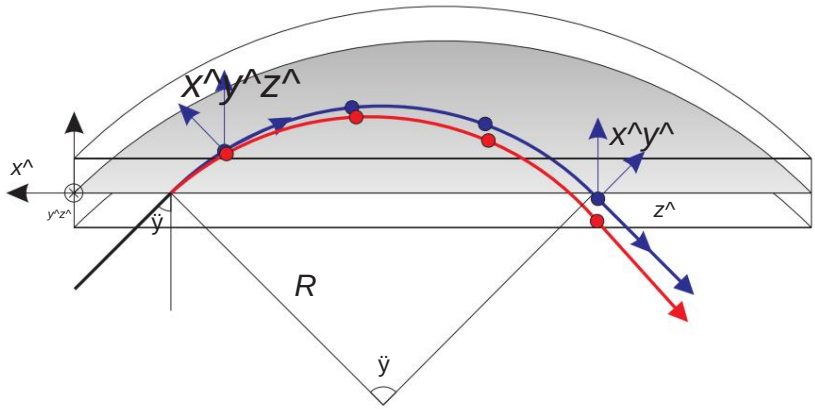

Figure 1.9:
Coordinate systems and segment magnet: The coordinate system moving with the target path (blue) forms the basis for all particle coordinates (red: particle path deviating from the target path), which are sensibly specified relative to the target particle. The coordinates of a particle in six-dimensional phase space are therefore ÿ ÿÿ ÿÿ ÿ ÿ.
With the segment magnet, the entry and exit takes place with the pole edge angle ÿ, the deflection angle is ÿ and the bending radius is ÿ.
The black coordinate system is intended for the coordinates of the magnetic field. The ÿÿ-axis protrudes into the plane of the drawing or into the interior of the magnet.

The RTM with two 180ÿ deflection magnets was already mentioned in 1946 [8]; the flexible arrangement of the deflection magnets allows, for example, the installation of an HF linac and individual focusing elements. In the case of the STM, the entry and exit angles in the deflection magnets are perpendicular to the face of the magnet, so the vertical defocusing effects of the real fringe field are smaller here than with polytrons *(N* > 1) with oblique pole edge angles *ÿ* [14].

The greatest distance between the nominal orbits of two adjacent orbits in the STM is caused by the transverse dispersion and is $n \cdot \ddot{y}/\ddot{y}$. Thus the distance at an acceleration frequency $\ddot{y} = c/\ddot{y}HF$ = 2.45 GHz for *n* = 1 is about 3.9 cm. This distance should always be a few centimeters, for example to be able to install correction magnets on the dispersion tracks [11].

The flight distances in an RTM increase with increasing energy, so that at

RTM3 the first circuit is already about 25 m long. This means that angle errors of *ÿx* ÿ 1 mrad can lead to position errors of *ÿx* ÿ 25 mm after just one revolution if no precautions are taken by focusing. Nevertheless, only small local deviations from the target magnetic field can be tolerated: At MAMI, the magnets are corrected by surface correction coils in such a way that for the deviations |*ÿB/ B*| ÿ 10ÿ4 can be maintained. Then mechanically "small" correction magnets on the dispersion orbits are sufficient to compensate for the remaining deflection errors (typically |*ÿxÿ* | < 1 mrad). In addition, this ensures for the longitudinal dynamics that there are no "jumps" in the path length, which in turn would cause non-correctable changes in the target phase ÿtarget [11].

1.3.1 Focusing the beam

To minimize the effects of position and angle errors, the beam must be focused. Then a beam deviating from the target path leads to a so-called
Betatron vibration around the target path specified by position monitors.

Various methods can be used to focus a beam
classified as "weak focus" and "strong focus".

“Weak focusing” has been known since the early days of cyclotrons and betatrons and can be observed with both homogeneous and inhomogeneous deflection magnets (see Figure 1.10). The "weak focusing" of a homogeneous deflection magnet takes place in the deflection plane, there is no focusing effect perpendicular to it. However, a superimposed gradient can also cause weak vertical focusing [14]. However, this focusing is very limited and not flexible, since it should deflect and focus horizontally at the same time and also focus vertically, which, however, has fundamental limits (Earnshaw Theorem).

Stronger and more flexible focusing can be achieved by alternating gradients ("alternating gradient"), because changing the gradient first focuses in one (eg horizontal) plane and then vice versa. If the distance between the gradient changes is smaller than the individual focal length, then this system has a focusing effect in *both* planes (eg focusing with a quadrupole doublet). Normally, single quadrupole magnets are used in “hard focusing”, but solenoid magnets can also be used.

Homogeneous deflection magnets

In a homogeneous magnetic field that is perpendicular to the accelerator plane, there is no vertical focusing. In the horizontal there is a focal point for parallel starting rays *(ÿx = 0, ÿx* = 0), which is also the reversal point of the ray (see Figure 1.10).

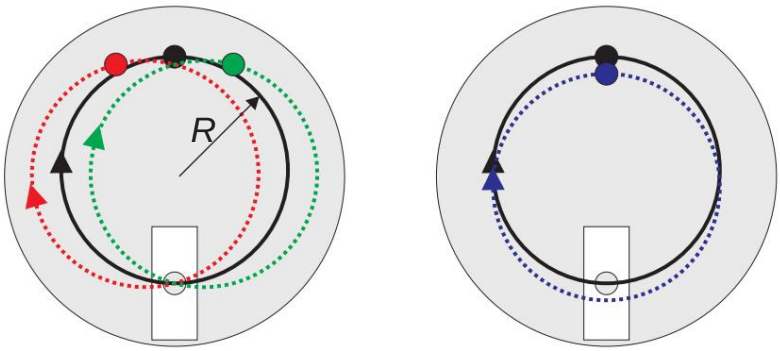

Figure 1.10: Weak focusing

in a homogeneous magnetic field: For magnetic fields ÿÿ ÿ ÿÿÿ ÿÿ ÿ ÿÿ perpendicular to the accelerator plane (ÿ/ÿ plane), the target path is a circular path (black). The weak focusing means that the beam always returns to the starting point (red and green) despite angular errors (ÿÿÿ ÿÿ ÿ, left) or for spatial errors (ÿÿ ÿÿ ÿ, right) there are two focal points. There is no focusing in the ÿ plane parallel to the magnetic field.

fringing effects

Due to fringe field effects, however, the magnetic field is only homogeneous and parallel to the y-axis inside a magnet ; at the pole edges, field components in the z-direction must be expected (Figure 1.9). In principle, this field component leads to a negative vertical focal length *fy* [7, 11]:

$$\frac{1}{f_y} = \frac{1}{R_2}\left[\int_{-\infty}^{0} \frac{\partial B}{\partial z}(z)\,dz - \frac{1}{B_0}\int_{-\infty}^{0} \frac{\partial B}{\partial z}(z)\,dz \int_{-\infty}^{z} \frac{\partial B}{\partial z}(z)\,dz + \frac{2}{3}\frac{1}{B_0^2}\int_{-\infty}^{0} \left(\frac{\partial B}{\partial z}(z)\right)^2 dz + \ldots\right] \tag{1.8}$$

with the orbit radius *R* in the homogeneous magnetic field B0. The boundary field extends from *ÿd* to 0 in the z-direction. Bÿ here is the derivative dB/dz. However, the defocusing can be compensated for by a suitable choice of the field curve *B(z)* in the peripheral field area . The opposing field strip according to Babiÿ and Sedlaÿek [7, 22] has prevailed as a solution for the RTM : In front of the homogeneous main field B0 there is an opposing field with Brev that is narrow in the z-direction . ÿ *ÿ0.2* B0 [23] . In this way, the vertical defocusing can be compensated for in the desired manner.

The Bz components have a much stronger effect if, in the case of the 90ÿ segment magnets, the beam does not enter and exit the magnetic field *perpendicularly ,* but rather at an angle. From the point of view of the beam, large Bx components are then present, which further increase the defocusing. Focal lengths of well under 1 m up to a few cm can be expected [6].

Field gradient perpendicular to the face of the magnet

Alternatively, instead of homogeneous magnets, a magnet with a gradient along the z-axis can be used to control the vertical defocusing - so-called "combined function" magnets. With increasing energy, the beam penetrates deeper and deeper into the magnet up to the reversal point zmax,i of orbit *i* . Therefore, for each additional orbit *j* with *j* > *i,* the field profile *B(z)* can be iteratively developed in the range between zmax,i < *z* < zmax,j without affecting the properties of the previous orbits.

An exponential decay is optimal, since the vertical image then becomes achromatic [23, 24]. With this procedure, the field gradient has been developed – taking into account the production techniques – in such a way that the vertical defocusing is compensated for practically over the entire energy range (Figure 1.11). The average remaining focal length is about 150 m, which can easily be compensated for by the quadrupoles on the linac axes [25].

The result is a magnet with a field gradient whose horizontal and vertical mapping corresponds to a drift path, but whose length is energy-dependent (Figure 1.12) [20, 26].

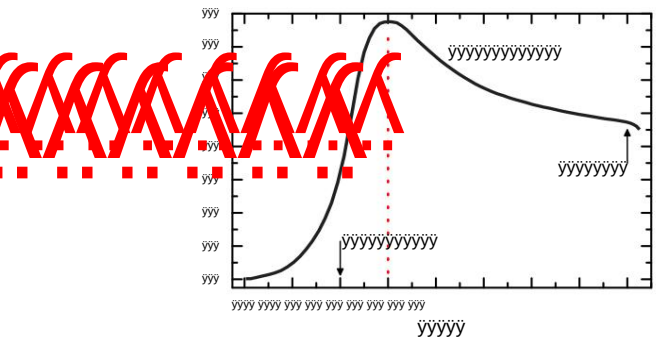

Figure 1.11:
Magnetic field versus distance to the pole edge (ÿÿ-axis) of an HDSM dipole [27].

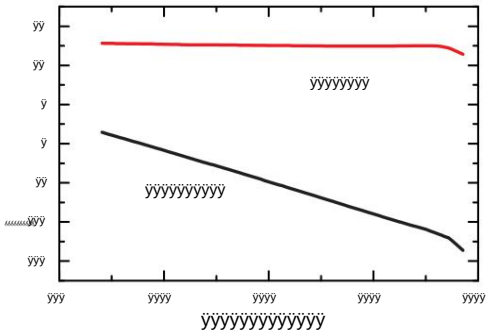

Figure 1.12:
Horizontal and vertical drift distances of a ÿÿÿÿ deflection system [27].

Taking Equation 1.7 into account , this macroscopic field gradient leads to the fact that the constant magnetic field *B* must be replaced by *ÿBÿ* < *B.* The reducing effect of the gradient increases from iteration *i* to iteration *j* such that ÿÿBÿj < ÿÿBÿi for *j* > i. But Equation 1.7 must be satisfied for all iterations, causing the target energy gain to decrease in the same way. With the right choice of target energy gain and phase, the inherent phase focus automatically leads to a continuous course of the acceleration. Nevertheless, the longitudinal stability needs to be examined more closely (Section 1.4). The field gradient optimized for vertical imaging requires that the energy gain of about 16.8 MeV at the shot energy

around 14 MeV at reject energy decreases; still around 17%, which is shown in Figure 1.13 [26].

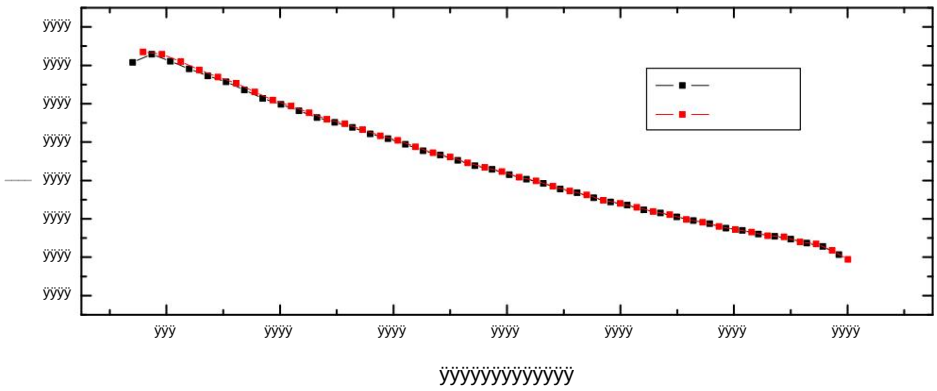

Figure 1.13:
Desired energy gain in HDSM: The field gradient requires the energy gain to decrease from around 17% over the course of acceleration.

Advantages of the telecentric segment magnet

Telecentricity enables the deflection system to be handled comparatively easily during operation , because essentially only drift paths need to be taken into account.

Because the deflection magnets have the desired telecentric properties, focusing is ideally done exclusively by quadrupoles on the linac axes7, as is the case with the STMs on MAMI. Various other focusing schemes are also discussed in detail in [26] and rejected compared to this simple scheme because they have no fundamental advantages over the method outlined.

1.3.2 Longitudinal Focusing

The combination of recirculation with longitudinal dispersion and a linac has a longitudinal focusing effect, since relativistic electrons *(v* ÿ c) with an energy deviation ÿE > 0 fly a slightly longer path through the longitudinal dispersion compared to the target particle and thus arrive at the HF resonator somewhat later. If the phase of the high-frequency is chosen so that the target particle lies on the falling edge, the electron with *ÿE* > 0 is accelerated somewhat less strongly by the HF and approaches the target particle in the next orbit, ie it follows a so-called synchrotron oscillation

7The focal length of a quadrupole magnet increases ÿ E, while that of a doublet increases with ÿ E2, so that doublet focusing decreases drastically with increasing energy. This effect is unproblematic because the energy is only roughly doubled with the HDSM.

around the target phase ÿ. Figure 1.2 already shows the effect of phase focusing; the theoretical background is explained in Section 1.4 .

Choice of target phase

An electromagnetic wave (or the electric field) is:

$$E\ddot{y}\ (\ddot{y}x,\ t) = E\ddot{y}0\ \text{ei}\ (\ \ddot{y}\ k\ddot{y}x\ \ddot{y}\ddot{y}\text{HFt}) = E\ddot{y}0\ \text{ei}\ddot{y}\ \_ \tag{1.9}$$

Since a standing wave forms in the (stationary) resonator, oBdA $k\ddot{y}x = 0$ and thus $\ddot{y} = \ddot{y}\ddot{y}$HFt. Therefore, in this notation, the phase $\ddot{y}$ for a particle with $\ddot{y}E > 0$ is *smaller* (or more negative) than that of the target particle due to longitudinal dispersion. The target energy gain ÿESoll of a single resonator or a linac is:

$$\ddot{y}\text{ESoll} = eU0\ \cos(\ddot{y}\text{soll}) \tag{1.10}$$

with ÿset < 0 in this convention. The target phase of the RTMs is therefore always negative.

1.4 Periodic Systems: Fundamentals of Longitudinal Dynamics

In a periodic system, it *must* be avoided that minor incorrect settings lead to deviations increasing beyond all limits (e.g. an energy gain $\ddot{y}E = \ddot{y}\ \ddot{y}$ESoll causes phase deviations $\ddot{y}\ddot{y}i = \ddot{y}$soll ÿ ÿi in a later cycle i).
The basics of longitudinal dynamics can be found in great detail in various works (e.g. [7, 14]) and are therefore only summarized here.

1.4.1 Description by the linear beam dynamics

With the means of linear jet dynamics , simple conditions can be formulated to check the stability , under which a periodically stable acceleration can take place. This will be shown later using the example of the longitudinal phase space *(ÿÿ, ÿE) .*

The derivation of the matrix formalism used for this from the Hamilton-Lagrange formalism and the vector potentials of the various accelerator components can be found in numerous publications [14]. Here follows a short summary of the original derivation [20].

1.4.2 Matrix formalism of jet dynamics

The motion of a single electron in external electromagnetic fields is described by the Hamiltonian *H(ÿv)* with *ÿv = (ÿx, ÿpx, ÿy, ÿpy, ÿ, ÿE, ÿz)* , where *ÿx, ÿy* , *ÿpx* and *ÿpy* are the local particle coordinates or the impulses related to the target particle and further *ÿÿ* and *ÿE* determine the phase and energy deviation.
The coordinate *z* corresponds to the distance covered along the target path and is “fixed” for highly relativistic particles with the phase *ÿ* or the deviations *ÿÿ* .

With a matrix S

$$S = \begin{pmatrix} 0 & 1 & 0 & 0 & 0 & 0 \\ -1 & 0 & 0 & 0 & 0 & 0 \\ 0 & 0 & 0 & 1 & 0 & 0 \\ 0 & 0 & -1 & 0 & 0 & 0 \\ 0 & 0 & 0 & 0 & 0 & 1 \\ 0 & 0 & 0 & 0 & -1 & 0 \end{pmatrix} \tag{1.11}$$

the movement of a particle is calculated from the Hamilton function:

$$\frac{d\ddot{y}v}{dz} = S \frac{\ddot{y}H}{\ddot{y}\ddot{y}v} \tag{1.12}$$

If only the Jacobian matrix J of *H(ÿv)* is taken into account, a solution is possible by integration over the distance *z :*

$$\ddot{y}v(z) = \ddot{y}v(0) + \int_0^{\ddot{y}z} SJ(s)\ddot{y}v(s)ds \tag{1.13}$$

For a J that is independent of *z* (ie for a drift path, for a movement in a homogeneous magnetic field, etc.), the following applies in particular

$$\ddot{y}v(z) = eSJ\, z\, \ddot{y}v(0) = M(z)\ddot{y}v(0) \tag{1.14}$$

where *M(z)* in the linear beam optics then the above mentioned section of the accelerator describes.

For a real beam guidance consisting of *n* individual such sections, which here are denoted by *i* ÿ [1, n], the solution for ÿÿv(z) is therefore given:

$$\ddot{y}v(z) = Mn \cdots Mi \cdots M2\, M1\, \ddot{y}v(0) \tag{1.15}$$

In the case of the longitudinal phase space, ÿv(0) ÿ (ÿÿbefore, ÿEbefore)T and analogously ÿv(z) ÿ (ÿÿafter, ÿEafter)T. The transformation matrix M is the product of the matrices *Mi.* Equation 1.15 can then be written as follows:

$$\begin{pmatrix} \ddot{y}\ddot{y}after \\ \ddot{y}Eafter \end{pmatrix} = M \cdot \begin{pmatrix} \ddot{y}\ddot{y}before \\ \ddot{y}Ebefore \end{pmatrix} \tag{1.16}$$

In a recirculating accelerator, a sequence of accelerator components is flown through several times. The smallest repetitive sequence is called *the unit cell ,* which can be used to characterize the longitudinal dynamics of a microtron.

The development of the longitudinal phase space consisting of phase and energy deviations *ÿÿ* and *ÿE* is essentially determined by the magnetic field of the deflection magnets and by the acceleration distances. Equation 1.17 thus describes the transformation of a circuit *i* consisting of a linac *Li* and a deflection system *Di:*

$$\begin{pmatrix} \ddot{y}\ddot{y}_{after} \\ \ddot{y}E_{after} \end{pmatrix} = D_i\, L_i \begin{pmatrix} \ddot{y}\ddot{y}_{before} \\ \ddot{y}E_{before} \end{pmatrix} \tag{1.17}$$

In the explanations that now follow, the circulation index *i* is omitted since *i* has no special function here. In the case of the DSM, however, the corresponding matrices also change as a result of the desired phase shift .

dipole matrix

The matrix D of the dipole acts as an energy-dependent drift path: the energy is not changed, only the phase deviation is subject to an energy-dependent transformation. For this purpose, the length of the drift with the matrix element D12 is selected in such a way that an "energy offset" ÿE corresponding to the target energy gain *ÿESoll* = eU0 cos (ÿsoll) leads to a phase change of *n* 360ÿ or *n* 2ÿ in order to fulfill the coherence condition :

$$D = \begin{pmatrix} 1 & \dfrac{n\,2\ddot{y}}{eU0\cos(\ddot{y}set)} \\ 0 & 1 \end{pmatrix} \ddot{y} \tag{1.18}$$

The sign of D12 takes into account the choice of the desired phase (ÿSoll < 0) defined in Section 1.3.2, since *ÿE* < 0 means a shorter transit time and the electron must therefore experience an acceleration greater than ÿESoll .

linac matrix

The matrix L of the linac, on the other hand , should not change the phase deviation *ÿÿ* because the electrons are relativistic and the linac is designed for *v* = *c* . However, a phase deviation *ÿÿ* leads to a different energy gain:

$$\ddot{y}E = \ddot{y}E_{Soll} + \ddot{y}E_{nach} = eU0\cos(\ddot{y}soll + \ddot{y}\ddot{y}) \tag{1.19}$$

In this notation, a linac behaves in a fundamentally non-linear manner, because in this expression the phase deviation *ÿÿ* appears as an argument of the cosine function. To the behavior

To be able to easily investigate the longitudinal dynamics, a linearization makes sense:

$$\begin{aligned} \ddot{y}Enach = \ddot{y}E \ddot{y} \ddot{y}Eset = \\ eU0 \cos(\ddot{y}set + \ddot{y}\ddot{y}) \ddot{y} eU0 \cos(\ddot{y}set) \\ \ddot{y} \ddot{y}eU0 \sin(\ddot{y}set) \ddot{y}\ddot{y} \end{aligned} \tag{1.20}$$

Here the expression in the last line of Equation 1.20 was approximated by the time derivation of the field profile, which is continued with the matrix element L21 :

$$L = \begin{pmatrix} 1 & 0 \\ \ddot{y} \ddot{y}eU0 \sin(\ddot{y}setpoint) & 1 \end{pmatrix} \tag{1.21}$$

The effect of L corresponds to focusing.

Acceleration approximated as a linear mapping

Because both matrices do not change at all (RTM, homogeneous magnetic field) or only slightly (DSM, field gradient) from one revolution to the next , one revolution can be viewed as an elementary cell of the periodic acceleration process. The entire acceleration process from cycle 1 to *n* is then described by the matrix product:

$$\ddot{y} \ddot{y}\ddot{y}En \ddot{y} = Dn \text{ Ln Dn } \ddot{y} \text{ 1 Ln } \ddot{y} \text{ 1} \quad \ldots \quad \text{D2 L2 D1 L1 } \ddot{y} \ddot{y}\ddot{y}1 \ddot{y}E1 \tag{1.22}$$

1.4.3 Stability, intrinsic ellipse and resonance phenomena

Stability in the sense mentioned requires that the transformation matrix M of the unit cell corresponds to a special similarity mapping (or a rotational stretching) with eigenvalues $|\ddot{y}| = e^{\pm i\ddot{y}}$ and corresponds to the angle of rotation ÿ. Since, according to Liouville's theorem, the volume of phase space under the action of conservative forces[8] is a conserved quantity , the following applies:

$$\det(M) \ddot{y} 1 \tag{1.23}$$

If both conditions are fulfilled, the repeated application of the transformation matrix M does not lead to an unlimited increase in the input deviations *ÿÿ0* and ÿE0, but the deviations describe points on the so-called eigenellipse from revolution to revolution, which is called synchrotron oscillation (longitudinal) or betatron oscillation (transverse). is to be observed. The angle ÿ by which the points move on from revolution to revolution on this ellipse is the so-called longitudinal

8The static magnetic fields of the deflection magnets and the electric fields of the acceleration sections can be represented as a gradient of a potential [28].

Phase advance ÿ, which is often expressed as the operating point ("tune") q = ÿ/2ÿ .
Then the matrix U corresponds to the original matrix M:

$$U = \ddot{y}\cos(\ddot{y}) \quad \ddot{y}\ddot{y}\sin(\ddot{y}) \quad \ddot{y}\sin(\ddot{y}) \quad \cos(\ddot{y}) \quad \ddot{y}\ddot{y}\sin(\ddot{y}) \quad \ddot{y}\ddot{y} \quad M \tag{1.24}$$

The Twiss parameters ÿ, $\ddot{y}$ and $\ddot{y}$ are subject to the condition $\ddot{y}\ddot{y}\ \ddot{y}\ddot{y}2 = 1$ and can be determined from M by comparing the matrix elements . The Twiss parameters determine the area (acceptance), eccentricity and orientation (convergent/divergent) of the eigenellipse.

At the same time applies

$$\text{Trace}(U) \ddot{y} 2\cos(\ddot{y}) , \tag{1.25}$$

ie one can calculate the phase shift ÿ directly from the matrix M and recognize under which conditions the transformation is periodic and not resonant:

$$|\text{Track}(M)| \ddot{y} 2 \tag{1.26}$$

For an RTM this means:

$$\text{Track}(M_{RTM}) = \text{Track}(L\ D) = 1 \ddot{y}$$
$$eU0 \sin(\ddot{y}) + 1 \quad eU0 \cos(\ddot{y}) \quad 2\ddot{y}\tan(\ddot{y}) = 2 + n \tag{1.27}$$

The target phase ÿtarget can be determined from the phase advance ÿ:

$$\ddot{y}_{setpoint} = \arctan \ddot{y}\cos(\ddot{y}) \ddot{y} 1 \tag{1.28}$$

With |2 + n 2ÿ tan(ÿ) | ÿ 2, a periodic acceleration follows for $\ddot{y}32.5\ddot{y}$ ÿ $\ddot{y}$ ÿ 0ÿ in the case of an RTM with harmonic number n = 1. With a DSM, the matrix Di must be taken into account that the total energy gain of a complete circuit (with two linacs $\ddot{y}E)$ must produce a path length increase of 360ÿ per deflection system due to longitudinal dispersion. Therefore, in the previous derivation of the RTM, the expression $\ddot{y}E = eU0$ cos(ÿsoll) should be replaced by 2ÿE for the DSM:

$$\text{Spur}(M_{DSM}) = \text{Spur}(L\ D) = 1 \ddot{y}$$
$$eU0 \sin(\ddot{y}) + 1 \quad eU0 \cos(\ddot{y}) \quad \tan(\ddot{y}) = 2 + n\ \ddot{y} \tag{1.29}$$

A stable periodic acceleration is therefore possible for $\ddot{y}51.85\ddot{y}$ ÿ $\ddot{y}$ ÿ 0ÿ at n = 1 [6, 29]. This comparatively large stability range is at least partially required by the field gradient of the deflection magnets.

Figure 1.14 shows the transformation of the phase space in two examples different phase advances ÿ.

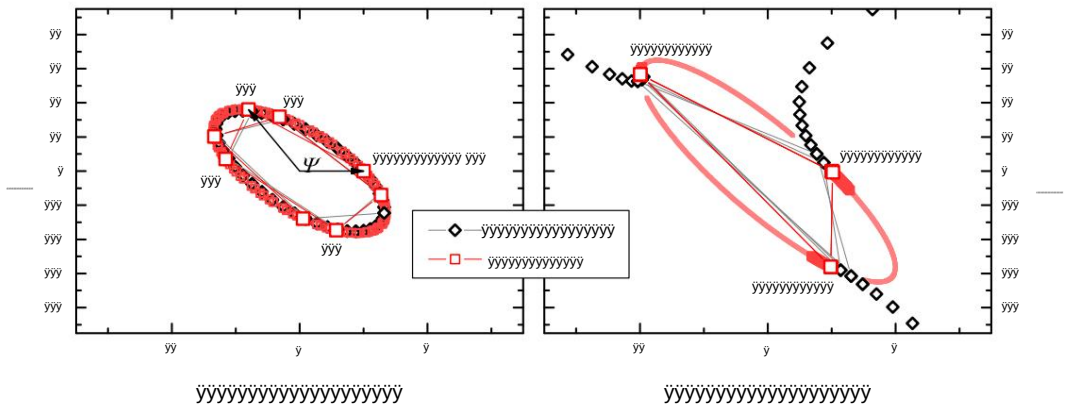

Figure 1.14:
Eigenellipse and resonance (RTM3): Transformation of a phase space from the starting point (+1ÿ, 0 keV) for 100 periods, the first eight are connected by lines. The eigenellipse is shown on the left with a phase advance ÿ of about 84.3ÿ (ÿÿ ÿ ÿÿÿÿ) . The differences between the complete calculation and the linearization are hardly noticeable. On the right, the eigenellipse is already very degenerate near ÿ ÿ 120ÿ (ÿ ÿÿ resonance). Here you can also see that only the full calculation shows the resonance peak (black diamonds); the linearization remains limited even after many orbits and eventually sweeps the entire edge, represented by the faint red curve.

"Adaptation" (matching) of the injected phase space

So far (and especially in Figure 1.14) only a punctiform ray has been considered, which describes the center of gravity of a real and extended bunch.

The distribution in the bunch extends over an area in phase space whose size is determined by the emittance9 of the beam. In order to distort the phase space as little as possible due to non-linearities (see above), the orientation of the injected phase space distribution should correspond to the system's own ellipse, otherwise the particles from the edge areas of the injected phase space will unnecessarily reach larger oscillation amplitudes. However, if the injected phase space is directed into the center of acceptance with the correct orientation, this is referred to as an "adapted" beam.

In order to achieve this, a suitable beam guidance is required in the transverse phase space , which rotates the phase space into the required orientation (eg divergent beam, parallel beam, etc.) with the help of quadrupole magnets and drift paths .

For the longitudinal phase space from *ÿÿ* and *ÿE* this means that by a Combination of acceleration and deflection system the orientation of the phase space

9The emittance describes the size of the spatial and momentum distribution.

can be adjusted to the proper ellipse. In the case of the HDSM, this adjustment in the injection beam guidance begins with the so-called “matching section” (MS, a short acceleration section, Figure 1.6), which the beam is intended to traverse in the vicinity of the zero crossing of the electric field. This does not change the mean energy of the beam, but the focusing effect of the gradient can be exploited to optimize the phase space upon arrival at the 4.9 GHz linac. Because that alone is not enough, the 4.9 GHz linac is injected during a *positive* phase. A small magnetic chicane extends the path length between the 4.9 GHz linac and the 2.45 GHz linac by about 10ÿ or 4.9 GHz, so that after this chicane the acceleration continues at phases *ÿ* < 0ÿ [20, 26]. Apart from that, the matching section is used later in the measurements to vary the injection energy by around ±1 MeV.

Synchrotron oscillation and optimization of longitudinal optics

A deviation *(ÿÿ, ÿE)* of the beam from the target particle leads to the beam describing an ellipse with the phase advance ÿ around the target particle. If several orbits *i* are considered, the phase deviations *ÿÿi* (as a projection of this ellipse onto the phase coordinates) can be measured that a synchrotron oscillation

$$ÿÿi = AS \sin(ÿ\, i + ÿ0) \tag{1.30}$$

describe. Both are shown in Figure 1.15. AS is the amplitude of the phase variations *ÿÿi* and ÿ0 the phase of the synchrotron oscillation when it first reaches the linac, which is linked to the phase of the particle on its own ellipse via the Twiss parameters [20].

Due to the more strongly varying injection phases *ÿ4.9* and *ÿ2.45* compared to the RTM, the Twiss parameters are also subject to larger fluctuations. Nevertheless, if the amplitude AS and phase ÿ0 are known , the approximate deviation *(ÿÿ0,* ÿE0) can be calculated and corrected if necessary. This is verified empirically in Section 4.5 and has since been used to optimize the HDSM.

resonances

If ÿ is too close to a rational quotient of *2ÿ* (e.g. ÿ = ÿ, ÿ = ÿ/2, ÿ = ÿ/3...), resonance phenomena can be observed that further amplify existing errors (see Figure 1.14). The matrix calculations can determine the phase shift ÿ well, but the resonance peaks cannot be made visible with this method.

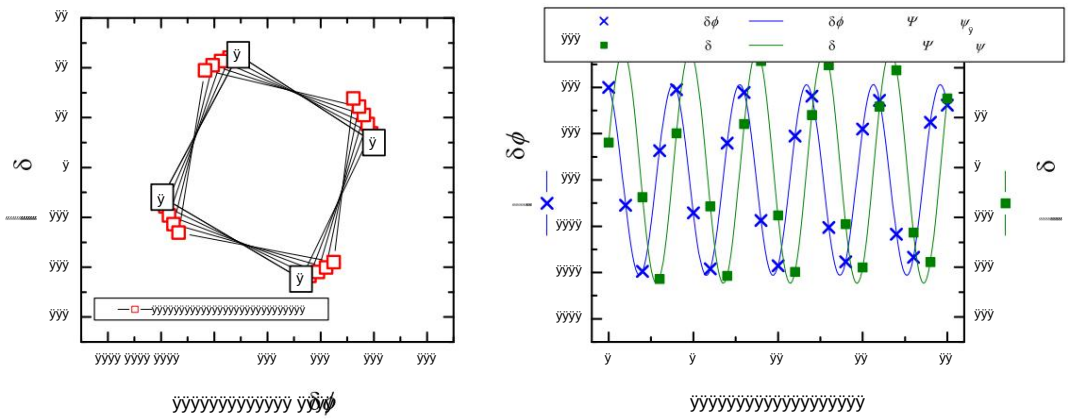

Figure 1.15:
Eigenellipse and synchrotron oscillation (injection HDSM 4.9 GHz: 9 MV, ÿÿ; 2.45 GHz: 9 MV, ÿÿÿÿ, linearized method): Analogous to Figure 1.14, the eigenellipse of the starting point (+1ÿ, 10th keV) for 20 “recirculations”, which is close to the ÿÿÿ resonance. On the right, this eigenellipse is shown as a synchrotron oscillation, to which a function ÿ ÿ ÿÿ ÿÿÿÿÿÿ ÿ ÿÿÿ was fitted for ÿÿÿ and ÿÿÿ. The measurable phase deviations ÿÿ are used in Section 4.5 to correct the injected beam with the help of amplitude ÿÿ ÿ ÿÿ and initial phase ÿÿ of the phase curve.

1.4.4 Influence of the magnetic field gradient on the longitudinal dynamics

In the coherence condition according to Equation 1.7, the gradient of the magnetic field leads to a smaller average magnetic field ÿBÿi that the beam experiences in a given revolution *i* . This in turn leads to a correspondingly smaller energy gain *ÿEi,* which , however, occurs automatically in the microtron due to the phase focusing, in that the target phase ÿSoll,i matching the correct energy gain is met. Therefore it will run through a certain interval *ÿi* ÿ [ÿ0, ÿ1] from injection to extraction .

With the ideally symmetrical DSM, both linacs are operated with the same HF amplitude U0 , and the bullet phase *ÿ* is also identical for both linacs.

Deviations from symmetry due to errors (e.g. HF amplitude, bullet phase, adjustment) mean that the bullet phases *ÿ* ÿ ÿ1, ÿ2 in both linacs can exhibit an offset *ÿ* ÿ= 0ÿ :

$$\ddot{y} = \ddot{y}2 \ddot{y} \ddot{y}1 \qquad (1.31)$$

For small *ÿ,* a mean and fictitious phase *ÿÿÿ* can be defined in order to fulfill the coherence condition with the resulting mean energy gain of both linacs [26]:

$$\cos(\ddot{y}1) + \cos(\ddot{y}2) = 2\cos(\ddot{y}\ddot{y}\ddot{y}) \qquad (1.32)$$

Because of the definition of *ÿ,* the easiest way to change its magnitude is to change the

Bullet phase ÿ2 in the second linac must be controlled, which must be considered more closely in the HDSM (especially in Chapter 4, Section 4.5.4).

1.4.5 Longitudinal stability of the DSM

In order to investigate the stability, different target phases ÿ1 and ÿ2 must be assumed in both linacs of the DSM. This means that the unit cell is no longer a half circuit, but must consider both linacs separately through M1 and M2 :

$$\begin{aligned}\text{Trace}(M) &= \text{Trace}(L2\ D\ L1\ D)\ n\ ÿ \\ &= ÿ\ 2 + \frac{\sin(ÿ2)}{\cos(ÿÿÿ)}\ ÿ\ ÿ\ 2 + \frac{n\ ÿ\ \sin(ÿ1)}{\cos(ÿÿÿ)}\ ÿ\ ÿ\ 2\end{aligned} \tag{1.33}$$

The result is no longer an interval of stable acceleration, but a two-dimensional surface over the phase coordinates ÿ1 and ÿ2 of the two linacs.
However, it is tacitly assumed here that *U0.1 = U0.2* applies to the RF amplitudes of Linac 1 and 2 .

The trace of Equation 1.33 is shown in Figure 1.16. There it becomes clear that deviations from symmetry (ÿ1,i ÿ= *ÿ2,i)* lead to the stable region near ÿ32.5ÿ *being* interrupted by a stop band, ie the stability diagram breaks up into two disjoint subregions. Apart from that, some longitudinal resonances have to be traversed, but this is unproblematic due to the small number of orbits in the critical area.

Stop band at ÿ32.5ÿ is problematic

For stable operation of the accelerator, it is therefore essential to ensure that
that the unstable region around the 1/2 resonance can be avoided, resulting in the following section is shown.

1.5 The harmonic double-sided microtron as a special case for MAMI-C

After the field profile *B(z)* optimized for transversal imaging properties requires a change in the target phase ÿSoll,i from one revolution *i* to the next, serious difficulties in the longitudinal dynamics /2 resonance in the last revolutions were to be expected when operating with two ÿ *ÿ32.5ÿ is reached,* which is due to the strong identical linacs . The reason for this is that *ÿ* focusing effect of the linacs L21 = *ÿeU0* sin(ÿi) .

However, if one considers the phase *ÿ* as a time coordinate, one finds that this matrix element is also affected by the frequency, because the energy deviation

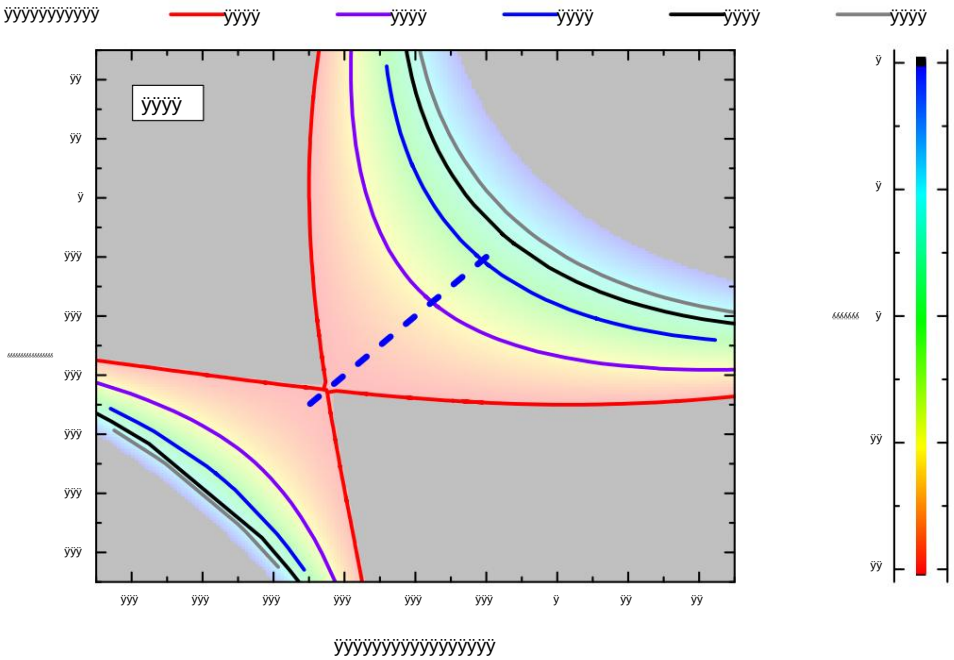

Figure 1.16:
Longitudinal stability range of the DSM: The colored area represents the range of longitudinally stable acceleration (representation is somewhat fainter to emphasize the resonance lines and the phase curve). The colors represent the trace of the unit cell matrix (grey ÿÿ unstable). Resonances that occur are represented by the solid colored lines.
The blue dotted line represents the planned phase progression [26]. In the DSM, they are area of the initial phase of ÿÿÿ-, ÿÿÿ- and even the ÿcrossed at a ÿÿ resonance. The stability ÿÿÿÿ has practically no extension at ÿ32.5ÿ . As a result, even small phase errors in this range lead to instabilities, which in turn can easily lead to beam losses.

ÿEafter after passing the linac (see Equation 1.20) depends on the phase *ÿ = ÿt* and thus also on the frequency *ÿ* (unless ÿEvor ÿ 0):

$$\begin{aligned} \text{ÿEnach} &= eU0\cos(\text{ÿ} + \text{ÿÿ})\ \text{ÿ}\ eU0\cos(\text{ÿ}) = \\ &eU0\cos(\text{ÿ}(t + \text{ÿt}))\ \text{ÿ}\ eU0\cos(\text{ÿt})\ dteU0 \\ &\text{ÿ}\quad \text{i.e.}\cos(\text{ÿt})\ \text{ÿt} = \text{ÿÿ}eU0 \\ &\sin(\text{ÿt})\ \text{ÿt} \end{aligned} \tag{1.34}$$

This corresponds to the fact that a linac with a higher frequency is described by a comparatively larger matrix element L21 ; lower frequencies reduce the matrix element accordingly (especially with the same reference phase L21,2.45 = / *2L21,4.9).* Figure 1.17 shows the two different frequencies (4.9 GHz and 2.45 GHz).[1]

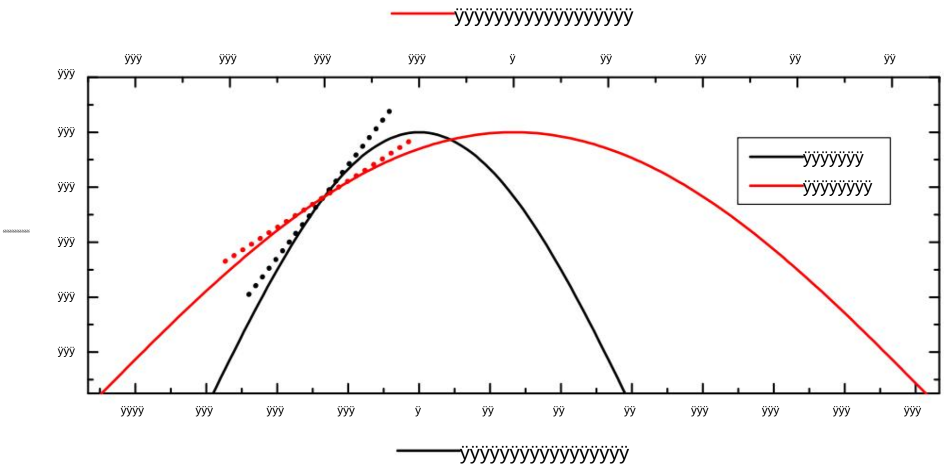

Figure 1.17:
Linac matrix element at two frequencies: The subharmonic frequency (red, 2.45 GHz) with the same target phase (here: ÿ ÿ ÿÿÿÿ) causes a halving of the focusing strength ÿÿÿ compared to due to the flatter gradient (see equation 1.34). 4.9 GHz, which is represented by the dotted lines.

In the further course, phase information usually refers to the fundamental frequency of the corresponding linac (eg *ÿ2.45* = ÿ32.5ÿ). In the case of ÿ, where both frequencies meet, the information is related to the basic frequency of the HDSM – i.e. 4.9 GHz.

1.5.1 Subharmonic margin

It is already noticeable in Figure 1.8 that omitting every second bunch means that in one of the two linacs only every second accelerating resonator is occupied with electrons. Exactly this situation applies to MAMI-C: The beam is injected into the 4.9 GHz system of the DSM with a repetition rate of 2.45 GHz.

Therefore, one of the two linacs can be operated at 2.45 GHz, which significantly improves longitudinal stability as intended.

Course of the target phase in the HDSM

The target phase changes of the two HDSM linacs from circuit to circuit are determined by the field gradient, since the coherence condition (equation 1.5) must be met. Only the injection phases *ÿ4.9* or *ÿ2.45* are initially arbitrary, but the stability criterion according to Equation 1.26 should be fulfilled for all orbits. Besides that

should the 1/2 resonance can be avoided with a sufficient safety margin10.

This problem is dealt with in detail in [26] . In summary, it should be noted here that the ideal phase curve in the 4.9 GHz linac is between 0ÿ and *ÿ32.5ÿ* (corresponding to the stable range of an STM); the phase curve in the 2.45 GHz linac should then be between *ÿ32.5ÿ* and a maximum of *ÿ51.85ÿ* .

1.5.2 Longitudinal stability of the HDSM

The symmetry of both linacs of the DSM is no longer present with the HDSM. Therefore, the elementary cell of the HDSM is the product of {180ÿ deflection, 4.9 GHz linac, 180ÿ deflection, 2.45 GHz linac} - i.e. a complete revolution -. The target energy gain *ÿE* must be divided between both linacs:

$$\ddot{y}E = \ddot{y}E4.9 + \ddot{y}E2.45 \tag{1.35}$$

$$\ddot{y}E4.9 = eU4.9\cos(\ddot{y}4.9) \tag{1.36}$$

$$\ddot{y}E2.45 = eU2.45\cos(\ddot{y}2.45) \tag{1.37}$$

In Equation 1.21 , the target energy gain of the respective linac must therefore be used in the expression for *Li* and the total energy gain in *Di.* Accordingly, the trace of the longitudinal circulation matrix reads:

$$\ddot{y}E\ \frac{2\ddot{y}\ddot{y}E2.45}{\tan(\ddot{y}2.45)\ \ddot{y}\ \ddot{y}E4.9}\ 2 + \frac{2\ddot{y}}{\ddot{y}E}\ \ddot{y}\ \ddot{y}\ddot{y}\ \frac{2\ddot{y}\ \ddot{y}\ 1 + \frac{\ddot{y}\ddot{y}E2.45}{\ddot{y}E}\tan(\ddot{y}2.45)\ \ddot{y}\ \ddot{y}}{\ddot{y}E}\ \ddot{y}\ \tan(\ddot{y}4.9) \tag{1.38}$$

Figure 1.18 shows the resulting stability area of the HDSM.

1.5.3 Consequence of target phase change in HDSM

The energy gain *ÿE* = ÿE4.9 + *ÿE2.45* causes a change in flight time from round to round, which is why the arrival time of the jet in both linacs changes by a similar amount. However, this change in flight time means that at different frequencies, for example, a 1ÿ phase change at 4.9 GHz corresponds to only 0.5ÿ at 2.45 GHz and the target phase change runs differently. Therefore Equation 1.31 has to be modified:

$$\ddot{y} = 2\ddot{y}2.45\ \ddot{y}\ \ddot{y}4.9 \tag{1.39}$$

ÿ is determined by the selection of the two entry phases *ÿ4.9* and *ÿ2.45 ;* So if you want to change *ÿ ,* for example, but leave the insertion phase in the 4.9 GHz linac, you can use the insertion phase in the 2.45 GHz linac to specify *ÿ .*

10The bunch length at MAMI is typically 2ÿ related to 2.45 GHz [30, 31]. The safety distance should correspond to this extension.

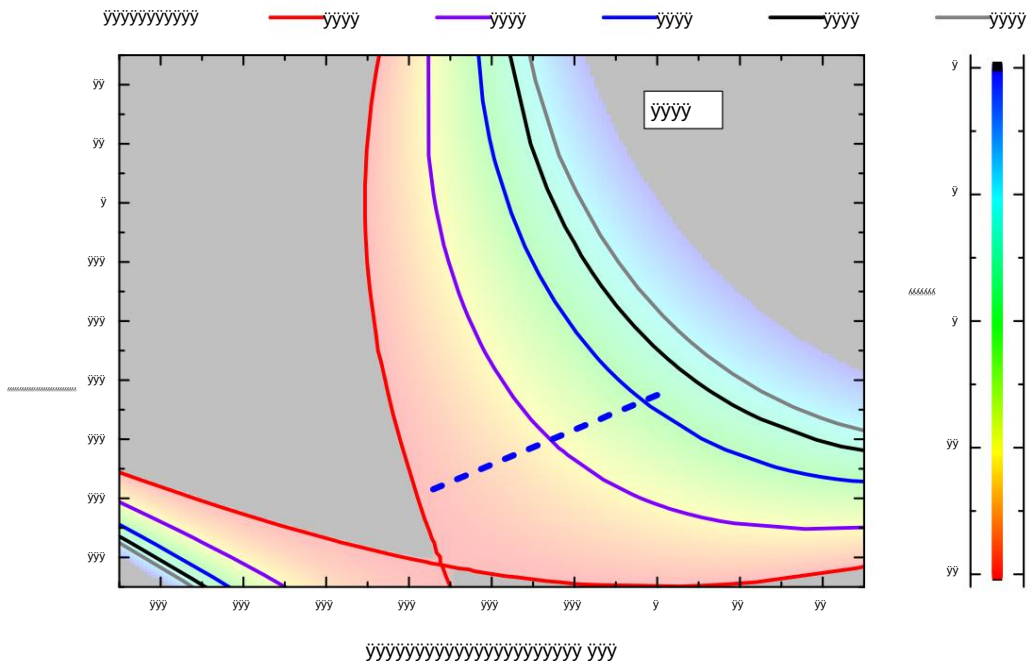

Figure 1.18:
Longitudinal stability area of the HDSM: Representation as in Figure 1.16. The phases ÿÿÿÿ and ÿÿÿÿ of the two linacs refer to the respective frequency.
The blue dotted line represents the planned phase progression [26]. The shot-in phases in the HDSM are 0ÿ (4.9 GHz) and ÿÿÿÿÿÿ (2.45 GHz) and only the ÿÿ and ÿÿ resonances have to be crossed. Investigations on this in Chapter 4.

Impact on the distribution of energy gain to both linacs

Ideally, the energy gain of one revolution *i* should be distributed evenly over both linacs - as with the DSM:

$$ÿEi = \text{eU4.9}\cos(ÿ4.9,i) + eU2.45\cos(ÿ2.45,i) \tag{1.40}$$

with

$$\text{eU4.9}\cos(ÿ4.9,i)\ ÿ\ eU2.45\cos(ÿ2.45,i) \qquad {}^{1}/_{2ÿEgg} \tag{1.41}$$

With a constant target phase *ÿi,* this is not a problem, but the ratio *ri* of the two energy gains *ÿE4.9,i* and ÿE2.45,i will change as a result of the target phase change .

That makes:

$$ri := \frac{ÿE4.9,i}{ÿE2.45,i} = \frac{\text{eU4.9}}{eU2.45} \cdot \frac{\cos(ÿ4.9,i)}{\cos(ÿ2.45,i)} \tag{1.42}$$

Since the ratio of the amplitudes *U4.9/ U2.45* is constant, only the second fraction with the cosine functions has to be considered. Substituted with Equation 1.39, the newly defined rÿi is :

$$r\ddot{y}i := \frac{\cos(\ddot{y}i)}{\cos((\ddot{y}i + \ddot{y})/2)} \tag{1.43}$$

However, this ratio of the two energy gains is *not* constant during acceleration due to the change in the target phase *ÿi .* Nevertheless, it should vary as little as possible in order to distribute the energy gain evenly over both linacs for all circuits. The choice of the entry phases *ÿ4.9* and *ÿ2.45* (and thus also of ÿ) should take this into account.

A favorable situation arises, for example, with identical amplitudes when the phase in the 4.9 GHz linac wanders from 0ÿ to ÿ30ÿ and simultaneously in the 2.45 GHz from ÿ20ÿ to ÿ35ÿ *(ÿ =* ÿ40ÿ), since in this case the quotient rÿi = *cos(ÿi)/* cos((ÿi + *ÿ)/ 2)* remains relatively constant in the corresponding phase interval (Figure 1.19, green curve). However, a value for *ÿ* ÿ ÿ70ÿ (injection phases *ÿ4.9* ÿ 0ÿ and *ÿ2.45* ÿ ÿ35ÿ) was planned, on the one hand to avoid the /2 resonance and on the other hand to follow the energy gain given by the field gradient. As a result, the energy gain for higher rotations is increasingly provided by the 4.9 GHz linac (rÿi runs from approx. 1.2 to 1.35).

This simplified consideration (here with identical amplitudes) is only intended to clarify that the distribution of the energy gain between the two linacs can be decisively influenced solely by the selection of the injection phases *ÿ4.9* and *ÿ2.45 .* Chapter 4 explores this further.

Figure 1.20 shows the influence of different HF amplitudes on the trace of the longitudinal matrix.

1.5.4 Consequences in operation and for jet dynamic investigations

The previous sections have made it clear that a double-sided microtron is well suited as a post-accelerator for MAMI. The field gradient of the deflection magnets greatly simplifies the vertical optics – on the other hand, it forces a non-negligible change in the target phase during acceleration. The harmonic double-ended microtron cleverly bypasses the critical longitudinal

1/2 resonance - first on paper.

The challenge now is to set this planned configuration on the real machine, examine it, optimize it and classify it using the stability diagram in Figure 1.18, for example.

Therefore, methods must be developed to record the relevant parameters as precisely as possible. The HF amplitudes *U4.9* and *U2.45* and the associated phases ÿ4.9,i and ÿ2.45,i of the individual revolutions i are particularly important.

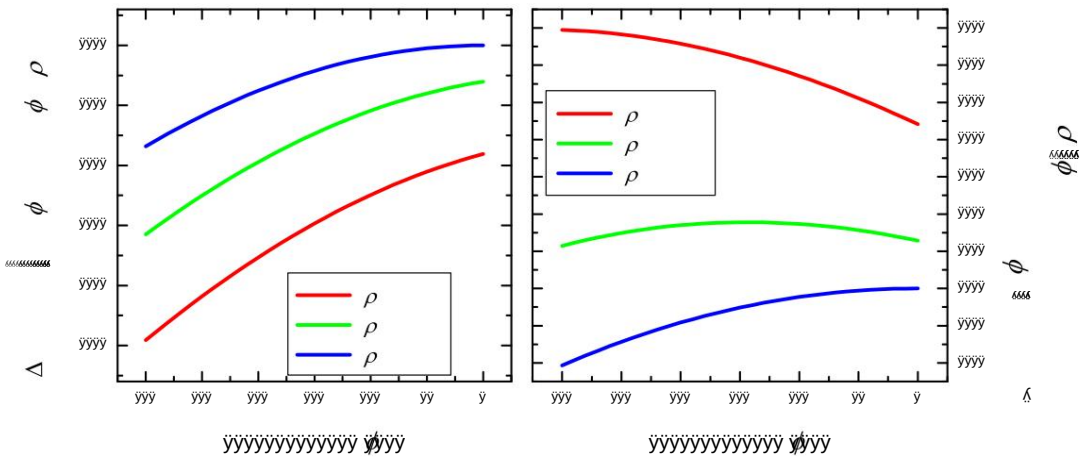

Figure 1.19:
Energy gain at two frequencies and target phase change: On the left, the sum of the energy gains of both linacs is shown in simplified form (ÿÿÿÿ ÿ ÿÿÿÿÿ ÿ ÿ) . For ÿ ÿ ÿÿ the relative energy gain decreases by about 9% - too little for the field gradient. For ÿ ÿ ÿÿÿÿ it decreases by about 15%, only for ÿÿÿÿ ÿ ÿ ÿ ÿÿÿÿ does it decrease by the amount of 17% required by the field gradient [26]. The ratio ÿ ÿÿ ÿ ÿÿÿÿÿÿÿ ÿÿÿÿÿÿ ÿ ÿÿÿÿ) is shown on the right. Ideally, ÿ ÿÿ should be as constant as possible during acceleration, so that the energy gain of one revolution is always distributed approximately equally between both linacs (e.g. green curve for ÿ ÿ ÿÿÿÿ) , but changing the energy gain requires ÿ.

1.5.5 Coupling between the phase spaces

In certain cases the phase spaces *(x,* xÿ), *(y,* yÿ) and *(ÿÿ, ÿE)* can be considered independently ; Liouville's theorem then applies separately in all three phase spaces. However, the individual subspaces can *no* longer be viewed independently of one another if couplings between the phase spaces occur . Instead, the entire phase space must then be transformed by a 6×6 matrix .

A simple example of this is the shot into the 180ÿ segment magnet of the STM with an angle error *ÿxÿ* ÿ= 0. This shortens or lengthens the distance in the magnetic field, so that a phase deviation *ÿÿ* can be observed after the magnet.
However, coupling can also be caused by many other effects and was also occasionally the subject of investigations in the RTMs on MAMI [20, 32].

In the HDSM model developed in Chapter 4, couplings between longitudinal and transverse phase space are deliberately neglected in order not to unnecessarily complicate the model, but the accessible transverse data (usually *x,* y) are also stored during the measurements carried out.
When analyzing the experiment, for example, those data can then be sorted out

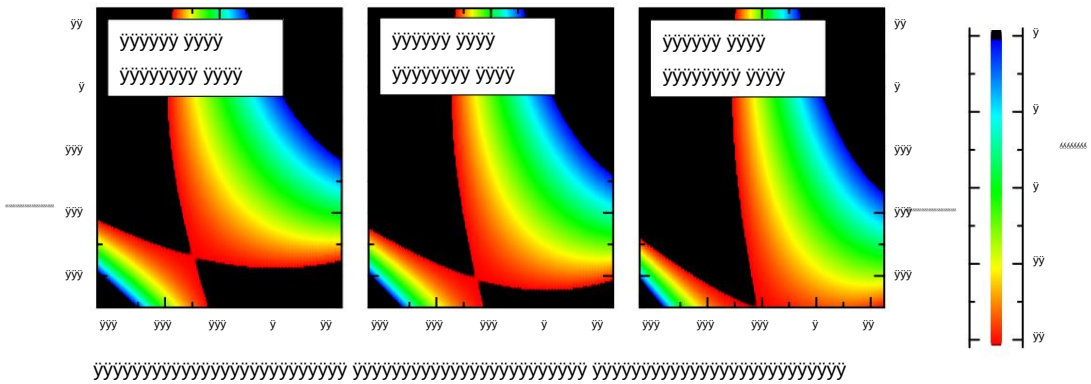

Figure 1.20:
Trace of the longitudinal transformation: Trace evaluated according to equation 1.38 for three different RF amplitude relations. The acceleration is not stable in the areas shown in black.

which show excessive transversal deviations from the nominal path.